Tellus (2006), 58A, 210–220
Printed in Singapore. All rights reserved

TELLUS

Transparent lateral boundary conditions for baroclinic waves II. Introducing potential vorticity waves

By A. McDONALD, *Met Éireann, Dublin, Ireland*

(Manuscript received 13 May 2005; in final form 16 September 2005)

ABSTRACT

Transparent boundary conditions are derived for two systems of linear equations which support potential vorticity waves as well as barotropic and baroclinic waves. The first system, the one-dimensional shallow water equations, supports potential vorticity and barotropic waves only and it is used to lay the foundations for the second system, the two-dimensional linearized hydrostatic primitive equations, which supports multiple baroclinic and potential vorticity waves. For each system of equations the derived boundary conditions are shown to be stable and accurate for practical integrations despite the presence of dispersive waves.

1. Introduction

In McDonald (2005), hereinafter called M05, transparent lateral boundary conditions were derived for two systems of linear equations which support baroclinic waves as well as barotropic waves. The purpose of this paper is to extend that work to systems of linear equations which also support potential vorticity waves by adding the Coriolis terms to the equations. The presence of these terms causes the waves to become dispersive and consequently the pivotal inverse transform becomes intractable. Fortunately, Engquist and Majda (1977) furnished a method for overcoming this difficulty. Their method gives rise to an increasingly accurate hierarchy of 'semi-transparent' boundary conditions, as is described in Section 2 for the one-dimensional shallow water model. In Section 3 it is shown that semi-transparent boundary conditions can be derived for a linearized multilevel model by transforming the equations into a set of shallow water equations each with its own effective depth. Using the methods described in Section 2 the boundary fields can be derived for each of these shallow water equations. Transforming these fields back to physical space completes the task of deriving semi-transparent boundary fields. These are then tested in a series of integrations and are shown to be stable and accurate.

2. A single-layer model

The complication caused by the introduction of the Coriolis terms is that the waves become dispersive. The purpose of this section is to examine the implications of this for the construction of transparent (in fact, now semi-transparent, as we shall see) boundary conditions. To do so, the simplest possible system that supports both gravity and potential vorticity waves is chosen: the one-dimensional shallow water equations. Baroclinic waves are excluded in order to discuss the complications caused by the dispersiveness of the waves with a minimum of algebraic clutter. More importantly, the boundary conditions for the multilevel model are derived in Section 3 by projecting the equations of motion into a series of shallow water equations each with a different gravity-inertia wave velocity. Therefore, the boundary conditions derived in this section will also be used in Section 3 for the multilevel model with a trivial re-definition of the gravity wave speed.

The equations are

$$\frac{\partial \eta}{\partial t} + \bar{u}\frac{\partial \eta}{\partial x} + H\frac{\partial u}{\partial x} = 0, \tag{1}$$

$$\frac{\partial u}{\partial t} + \bar{u}\frac{\partial u}{\partial x} + g\frac{\partial \eta}{\partial x} - fv = 0, \tag{2}$$

$$\frac{\partial v}{\partial t} + \bar{u}\frac{\partial v}{\partial x} + fu = 0, \tag{3}$$

where x and t are the space and time co-ordinates, and $g = 9.81$ is the gravitational acceleration, $\bar{u}$ is a constant advecting velocity, and $f = 10^{-4}$ is a constant Coriolis parameter. The field $\eta(x, t)$ describes the displacement of the fluid surface from its resting thickness, H. Lastly, $u(x, t)$ and $v(x, t)$ are the eastward and northward horizontal velocity components.

2.1. Derivation of the boundary conditions

Let $\mathbf{\Psi}$ be the vector (superscript 'T' denotes transpose)

$$\mathbf{\Psi} = (\eta, u, v)^T. \tag{4}$$

Corresponding author.
e-mail: aidan.mcdonald@met.ie
DOI: 10.1111/j.1600-0870.2006.00161.x

Taking the Laplace transform,

$$\hat{\mathbf{\Psi}}(x,s)=\int_0^\infty e^{-st}\mathbf{\Psi}(x,t)\,\mathrm{d}t, \tag{5}$$

of eqs. (1)–(3) and using property 15 on page 210 of Doetsch (1971) yields

$$s\hat{\eta}(x,s)+\bar{u}\frac{\partial\hat{\eta}(x,s)}{\partial x}+H\frac{\partial\hat{u}(x,s)}{\partial x}=\eta(x,0_+), \tag{6}$$

$$s\hat{u}(x,s)+\bar{u}\frac{\partial\hat{u}(x,s)}{\partial x}+g\frac{\partial\hat{\eta}(x,s)}{\partial x}-f\hat{v}(x,s)=u(x,0_+), \tag{7}$$

$$s\hat{v}(x,s)+\bar{u}\frac{\partial\hat{v}(x,s)}{\partial x}+f\hat{u}(x,s)=v(x,0_+), \tag{8}$$

or, in matrix form,

$$\begin{bmatrix}\bar{u}&H&0\\g&\bar{u}&0\\0&0&\bar{u}\end{bmatrix}\frac{\partial}{\partial x}\begin{bmatrix}\hat{\eta}\\\hat{u}\\\hat{v}\end{bmatrix}(x,s)+s\begin{bmatrix}1&0&0\\0&1&-f/s\\0&f/s&1\end{bmatrix}\begin{bmatrix}\hat{\eta}\\\hat{u}\\\hat{v}\end{bmatrix}(x,s)=\begin{bmatrix}\eta\\u\\v\end{bmatrix}(x,0_+), \tag{9}$$

or, symbolically,

$$\mathbf{A}\frac{\partial\hat{\mathbf{\Psi}}(x,s)}{\partial x}+s\mathbf{B}\hat{\mathbf{\Psi}}(x,s)=\mathbf{\Psi}(x,0_+). \tag{10}$$

Comparing eqs. (10) and (9) makes the definitions of $\mathbf{A}$ and $\mathbf{B}$ obvious. Multiplying across by $\mathbf{A}^{-1}$ yields

$$\frac{\partial\hat{\mathbf{\Psi}}(x,s)}{\partial x}+s\mathbf{A}^{-1}\mathbf{B}\hat{\mathbf{\Psi}}(x,s)=\mathbf{A}^{-1}\mathbf{\Psi}(x,0_+), \tag{11}$$

where

$$\mathbf{A}^{-1}=\frac{1}{\bar{u}(\bar{u}^2-gH)}\begin{bmatrix}\bar{u}^2&-\bar{u}H&0\\-\bar{u}g&\bar{u}^2&0\\0&0&\bar{u}^2-gH\end{bmatrix}, \tag{12}$$

and

$$\mathbf{A}^{-1}\mathbf{B}=\frac{1}{\bar{u}(\bar{u}^2-gH)}\begin{bmatrix}\bar{u}^2&-\bar{u}H&\bar{u}Hf/s\\-\bar{u}g&\bar{u}^2&-\bar{u}^2f/s\\0&(\bar{u}^2-gH)f/s&(\bar{u}^2-gH)\end{bmatrix}. \tag{13}$$

If a matrix $\mathbf{Q}$ can be found such that

$$\mathbf{Q}^{-1}\mathbf{A}^{-1}\mathbf{B}\mathbf{Q}=\mathbf{\Lambda}, \tag{14}$$

where $\mathbf{\Lambda}$ is a diagonal matrix, then its diagonal elements consist of the eigenvalues of $\mathbf{A}^{-1}\mathbf{B}$, and $\mathbf{Q}^{-1}$ consists of its left eigenvectors. Defining Y to be

$$Y=\left\{1+\frac{f^2}{s^2}\left(1-\frac{\bar{u}^2}{\bar{c}^2}\right)\right\}^{\frac{1}{2}}, \tag{15}$$

where $\bar{c}=\sqrt{gH}$, the three eigenvalues are

$$\lambda_\pm=\frac{1}{\bar{u}\pm\bar{c}}\pm\frac{\bar{c}(1-Y)}{\bar{u}^2-\bar{c}^2};\quad \lambda_{pv}=\frac{1}{\bar{u}}, \tag{16}$$

corresponding to the two gravity-inertia waves and the potential vorticity wave, respectively. The left eigenvectors associated with these eigenvalues are, respectively,

$$\mathbf{l}_\pm=n_\pm(s)\left(g,\ \pm\bar{c}Y,\ \frac{f}{s}\bar{u}\right);\quad \mathbf{l}_{pv}=n_{pv}(s)\left(\frac{\bar{u}}{H}\frac{f}{s},\ \frac{f}{s},\ 1\right), \tag{17}$$

where $n_\pm(s)$ and $n_{pv}(s)$ are arbitrary normalization factors. Multiplying eq. (11) by $\mathbf{l}_k$ yields an equation, ($\mathbf{l}_1=\mathbf{l}_+$, $\mathbf{l}_2=\mathbf{l}_{pv}$, $\mathbf{l}_3=\mathbf{l}_-$),

$$\frac{\partial\mathbf{l}_k.\hat{\mathbf{\Psi}}(x,s)}{\partial x}+s\lambda_k\mathbf{l}_k.\hat{\mathbf{\Psi}}(x,s)=\mathbf{l}_k.\mathbf{A}^{-1}\mathbf{\Psi}(x,0_+), \tag{18}$$

whose solution is, see page 21 of Ince (1956),

$$\mathbf{l}_k.\hat{\mathbf{\Psi}}(x,s)=\mathbf{l}_k.\hat{\mathbf{\Psi}}(x_0,s)e^{-s\lambda_k(x-x_0)}+e^{-s\lambda_k x}\int_{x_0}^{x}\mathbf{l}_k.\mathbf{A}^{-1}\mathbf{\Psi}(\xi,0_+)e^{s\lambda_k\xi}\,\mathrm{d}\xi. \tag{19}$$

Consider the λ_+-wave. If the arbitrary normalization factor, $n_+(s)$, is chosen to be 1, and it is assumed that terms of order f/s or higher make only a small contribution to the inverse Laplace transform of eq. (19) the result is, see property 9 on page 209 of Doetsch (1971),

$$[g\eta+\bar{c}u](x,t)=[g\eta+\bar{c}u]\left(x_0,t-\frac{x-x_0}{\bar{u}+\bar{c}}\right)+In_+^0. \tag{20}$$

If, on the other hand, $n_+(s)=s$ and it is assumed that terms of order $(f/s)^2$ or higher make only a small contribution to the inverse Laplace transform of eq. (19) the result is

$$\left[\frac{\partial(g\eta+\bar{c}u)}{\partial t}+f\bar{u}v\right](x,t)=\left[\frac{\partial(g\eta+\bar{c}u)}{\partial t}+f\bar{u}v\right]\left(x_0,t-\frac{x-x_0}{\bar{u}+\bar{c}}\right)+In_+^1. \tag{21}$$

Here In_+^k represents the contribution to the solution from the initial state, which is not of interest as far as deriving boundary conditions is concerned. In principle, this procedure can be continued, deriving solutions containing higher and higher time derivatives.

Consider a region of integration defined by $0\le x\le L$, and $\bar{u}+\bar{c}>0$, then what eq. (21) says is that if, at any time t the combination of fields on the right-hand side is non-zero at $x_0=0$, then $x/(\bar{u}+\bar{c})$ seconds later this non-zero value will have been transported to the position x in the interior at a speed $(\bar{u}+\bar{c})\,\mathrm{ms}^{-1}$. Thus, to prevent this gravity-inertia wave from entering the region it is essential to maintain the condition $[\partial(g\eta+\bar{c}u)/\partial t+f\bar{u}v](0,t)=0$ throughout the integration . By the same token, in a nested integration, if boundary fields are being supplied from an external 'host' model, designated by the superscript h, and they are such that $[\partial(g\eta^h+\bar{c}u^h)/\partial t+f\bar{u}v^h](0,t)\neq 0$ then this gravity-inertia wave will enter the integration area. If $\bar{u}+\bar{c}<0$

the reasoning is the same except that it applies to the boundary at $x = L$.

If $n_{pv}(s) = 1$ and it is assumed that terms of order f/s or higher make only a small contribution to the inverse Laplace transform of eq. (19) the result is

$$v(x,t) = v\left(x_0, t - \frac{x - x_0}{\bar{u}}\right) + In^0_{pv}. \tag{22}$$

If $n_{pv}(s) = s$ then, to all orders of f/s,

$$\left[\frac{\partial v}{\partial t} + f\left(u + \frac{\bar{u}}{H}\eta\right)\right](x,t) = \left[\frac{\partial v}{\partial t} + f\left(u + \frac{\bar{u}}{H}\eta\right)\right]\left(x_0, t - \frac{x - x_0}{\bar{u}}\right) + In^1_{pv}. \tag{23}$$

Substituting u from eq. (3) yields

$$-\frac{1}{\bar{u}}\left[\frac{\partial v}{\partial t} + f\left(u + \frac{\bar{u}}{H}\eta\right)\right] = \frac{\partial v}{\partial x} - \frac{f\eta}{H}, \tag{24}$$

the potential vorticity for the system of eqs. (1)–(3). That it is conserved following the parcel can be seen by taking $\partial/\partial x$ of eq. (3) and subtracting f/H times eq. (1).

Now, repeating the above arguments, if $\bar{u} > 0$, in a nested integration, in order to inject potential vorticity into the integration at $x = 0$ via a host model, put $v(t,0) = v^h(t,0)$ to lowest order. To all higher orders put $[\partial v/\partial t + f(u + \bar{u}\eta/H)](0,t)$ equal to its host model value. If $\bar{u} < 0$ the reasoning is the same except that it applies to the boundary at $x = L$.

2.2. *Time discretization of the boundary conditions*

In this section is described how to derive an order-consistent set of discretized boundary conditions. First, some definitions. Write

$$\hat{W}_k = (\mathbf{Q^{-1}}\hat{\mathbf{\Psi}})_k, \tag{25}$$

such that $\hat{W}_1$, $\hat{W}_2$ and $\hat{W}_3$ are associated with the λ_+, λ_{pv}, and λ_- waves, respectively. Then from eq. (17)

$$\mathbf{Q}^{-1} = \begin{bmatrix} g & \bar{c}Y & \frac{f}{s}\bar{u} \\ \frac{\bar{u}g}{\bar{c}^2}\frac{f}{s} & \frac{f}{s} & 1 \\ g & -\bar{c}Y & \frac{f}{s}\bar{u} \end{bmatrix}, \tag{26}$$

and its inverse is

$$\mathbf{Q} = \left[2\bar{c}Y\left(1 - \frac{\bar{u}^2}{\bar{c}^2}\frac{f^2}{s^2}\right)\right]^{-1} \times \begin{bmatrix} \frac{\bar{c}}{g}\left(Y + \frac{\bar{u}}{\bar{c}}\frac{f^2}{s^2}\right) & -\frac{2\bar{u}\bar{c}Y}{g}\frac{f}{s} & \frac{\bar{c}}{g}\left(Y - \frac{\bar{u}}{\bar{c}}\frac{f^2}{s^2}\right) \\ 1 - \frac{\bar{u}^2}{\bar{c}^2}\frac{f^2}{s^2} & 0 & -1 + \frac{\bar{u}^2}{\bar{c}^2}\frac{f^2}{s^2} \\ -\left(1 + \frac{\bar{u}Y}{\bar{c}}\right)\frac{f}{s} & 2\bar{c}Y & \left(1 - \frac{\bar{u}Y}{\bar{c}}\right)\frac{f}{s} \end{bmatrix}. \tag{27}$$

Consider the boundary at $x = 0$. Let there be l values of $\lambda > 0$. Thus the host values of $\hat{W}^h_1, \hat{W}^h_2, \ldots \hat{W}^h_l$ must be imposed and the remaining values of $\hat{W}^g_{l+1}, \ldots \hat{W}^g_K$ must be extrapolated from the interior, hence the superscript g, designating the nested 'guest' fields; $K = 3$, but the argument is quite general. Define

$$\hat{\mathbf{W}} = \left(\hat{W}^h_1, \ldots \hat{W}^h_l, \hat{W}^g_{l+1}, \ldots \hat{W}^g_K\right)^T, \tag{28}$$

then the boundary fields are given by

$$\hat{\mathbf{\Psi}} = \mathbf{Q}\hat{\mathbf{W}}. \tag{29}$$

Expand this as

$$\hat{\mathbf{\Psi}} = \mathbf{Q}^{(0)}\hat{\mathbf{W}}^{(0)} + \frac{f}{s}\left(\mathbf{Q}^{(1)}\hat{\mathbf{W}}^{(0)} + \mathbf{Q}^{(0)}\hat{\mathbf{W}}^{(1)}\right) + O\left(\frac{f^2}{s^2}\right), \tag{30}$$

where

$$\hat{\mathbf{W}}^{(i)} = [\mathbf{Q}^{-1}]^{(i)}\hat{\mathbf{\Psi}}. \tag{31}$$

The zero-order matrices $\mathbf{Q}^{(0)}$ and $[\mathbf{Q}^{-1}]^{(0)}$ are defined by setting $f/s = 0$ in eqs. (26) and (27). Also, the first-order matrices $\mathbf{Q}^{(1)}$ and $[\mathbf{Q}^{-1}]^{(1)}$ are defined by setting all except the terms proportional to f/s equal to zero. Dropping the $O(f^2/s^2)$ terms in eq. (30), multiplying by s, and transforming back yields the boundary fields

$$\frac{\partial \mathbf{\Psi}}{\partial t} = \mathbf{Q}^{(0)}\frac{\partial \mathbf{W}^{(0)}}{\partial t} + f\left(\mathbf{Q}^{(1)}\mathbf{W}^{(0)} + \mathbf{Q}^{(0)}\mathbf{W}^{(1)}\right). \tag{32}$$

The following simple discretization is used in the tests described later:

$$\Delta\mathbf{\Psi} = \mathbf{Q}^{(0)}\Delta\mathbf{W}^{(0)} + f\Delta t\left(\mathbf{Q}^{(1)}\mathbf{W}^{(0)}_{av} + \mathbf{Q}^{(0)}\mathbf{W}^{(1)}_{av}\right), \tag{33}$$

where for any field ϕ, $\Delta\phi = \phi^{n+1} - \phi^n$ and $\phi_{av} = (\phi^{n+1} + \phi^n)/2$.

In this derivation it has been assumed that it is permissible to regard f/s as a small parameter. Engquist and Majda (1977) furnish the theoretical justification. For an update, see Hagstrom (1999).

Remark: McDonald (2002) proposed that for $\bar{c} > \bar{u} > 0$, $g\eta + \bar{c}u$ and v be imposed at $x = 0$ for a two-dimensional barotropic model. This corresponds to dropping the first-order terms in eq. (30). From the point of view of this section, his boundary conditions are zero order for incoming waves and first order for outgoing waves. Notice however, that from a meteorological point of view, where the potential vorticity wave dominates, the effective level of accuracy of the incoming waves may be almost first order for the following reason. In the absence of gravity waves $\mathbf{l}_+.\hat{\Psi} = \mathbf{l}_-.\hat{\Psi} = 0$, implying $g\hat{\eta} + (f\bar{u}\hat{v}/s) = 0$ and $\hat{u} = 0$, which when substituted in eq. (25) yields

$$\hat{W}_{pv} \equiv \hat{W}_2 = \hat{v}\left(1 - \frac{f^2}{s^2}\frac{\bar{u}^2}{\bar{c}^2}\right). \tag{34}$$

Hence, in the absence of gravity waves, imposing v at inflow is a first-order condition. Of course, this argument breaks down if the guest model fields, or the host model fields that are being

used to drive the guest model, contain large amplitude gravity waves.

2.3. Extrapolations associated with the boundary conditions

A grid is used in which the u-fields are staggered from the η-fields and v-fields, with both the latter at the end points. The boundary conditions are imposed at $x = \Delta x/2$ and $x = L - \Delta x/2$, rather than at 0 and L in order to minimize extrapolations. The details are given for imposing the boundary conditions at $x = \Delta x/2$ only. Exactly the same logic applies at $x = L - \Delta x/2$.

The following are used for computing $\mathbf{W}^g$ at time level $n+1$. The fields η and v are extrapolated; $u(\Delta x/2, n+1)$ is a known quantity:

$$\Psi_1\left(\frac{\Delta x}{2}, n+1\right) = 0.5[3\eta(\Delta x, n+1) - \eta(2\Delta x, n+1)];$$
$$\Psi_2\left(\frac{\Delta x}{2}, n+1\right) = u\left(\frac{\Delta x}{2}, n+1\right);$$
$$\Psi_3\left(\frac{\Delta x}{2}, n+1\right) = 0.5[3v(\Delta x, n+1) - v(2\Delta x, n+1)]. \quad (35)$$

The following are used for computing $\mathbf{W}^g$ at time level n and for computing $\mathbf{W}^h$ at time levels n and $n+1$.

$$\Psi_1\left(\frac{\Delta x}{2}, n\right) = 0.5[\eta(0, n) + \eta(\Delta x, n)];$$
$$\Psi_2\left(\frac{\Delta x}{2}, n\right) = u(\frac{\Delta x}{2}, n); \quad (36)$$
$$\Psi_3\left(\frac{\Delta x}{2}, n\right) = 0.5[v(0, n) + v(\Delta x, n)].$$

Finally, once $\mathbf{\Psi}(\Delta x/2, n+1)$ has been re-constituted as a combination of interior and exterior fields, via eq. (29), η and v are then extrapolated to the boundary:

$$\Psi_m(0, n+1) = 2\Psi_m\left(\frac{\Delta x}{2}, n+1\right) - \Psi_m(\Delta x, n+1), \quad (37)$$

for $m = 1$ and 3.

2.4. Discretization of the equations of motion

For the spatial discretization the u-fields are staggered from the η- and v-fields, with both the latter at the end points. For the time discretization the leapfrog scheme is used. Thus, eqs. (1)–(3) are discretized as

$$\eta(i, n+1) = \eta(i, n-1) - \frac{\bar{u}\Delta t}{\Delta x}[\eta(i+1, n) - \eta(i-1, n)] - \frac{2H\Delta t}{\Delta x}\left[u\left(i+\frac{1}{2}, n\right) - u\left(i-\frac{1}{2}, n\right)\right], \quad (38)$$

$$u\left(i+\frac{1}{2}, n+1\right) = u\left(i+\frac{1}{2}, n-1\right) - \frac{\bar{u}\Delta t}{\Delta x}\left[u\left(i+\frac{3}{2}, n\right) - u\left(i-\frac{1}{2}, n\right)\right] - \frac{2g\Delta t}{\Delta x}[\eta(i+1, n) - \eta(i, n)] + f\Delta t[v(i+1, n) + v(i, n)], \quad (39)$$

$$v(i, n+1) = v(i, n-1) - \frac{\bar{u}\Delta t}{\Delta x}[v(i+1, n) - v(i-1, n)] - f\Delta t\left[u\left(i+\frac{1}{2}, n\right) + u\left(i-\frac{1}{2}, n\right)\right]. \quad (40)$$

where $x = i\Delta x$, $L = I\Delta x$, and $t = n\Delta t$. The boundary fields, $\eta(0, n+1)$, $v(0, n+1)$, $\eta(I, n+1)$, and $v(I, n+1)$, must be supplied. How to do this was discussed in Sections 2.2 and 2.3. A Robert (1966) filter is used to control the computational mode. Equations (38) and (40) are valid from $i = 1$ to $i = I - 1$. Equation (39) is valid from $i = 0$ (where a right derivative is used for the advection term) to $i = I - 1$ (where a left derivative is used for the advection term).

2.5. Testing the boundary conditions

In this section a practical demonstration is given of a potential vorticity wave being injected into the integration area while simultaneously two inertia-gravity waves radiate through the boundaries.

The parameters used were $\Delta x = 10$ km, $\Delta t = 9.0$ s, $\bar{u} = 50\ \mathrm{ms}^{-1}$, $gH = 300 \times 300\ \mathrm{m}^2\ \mathrm{s}^{-2}$. These result in $\bar{c} = 300\ \mathrm{ms}^{-1}$. Thus the two gravity-inertia waves have velocities of approximately $350\ \mathrm{ms}^{-1}$ and $-250\ \mathrm{ms}^{-1}$, typical of 'external' gravity waves, and the incoming potential vorticity wave is 'jet-like'.

Two sets of integrations were performed; one with $L = 1000$ km, $I = 101$, and a second 'host integration' with $L^h = 10\,000$ km, and $I^h = 1001$. The latter integration, whose boundaries are so far removed that no waves can travel to them and back to the boundary of the guest integration domain during the length of the integration, was used as the 'correct integration' with which the test integrations were compared. It was also used to furnish the boundary fields to inject the potential vorticity wave into the region of integration. The first-order boundary condition described by eq. (33) was used.

Defining a bellshape as

$$b_i\left(x, x_s, \bar{c}_i^0 t, \Gamma_s\right) = \exp\left[-\left\{\frac{\left(x - x_s - \bar{c}_i^0 t\right)}{\Gamma_s}\right\}^2\right], \quad (41)$$

where $\bar{\mathbf{c}}^0 = [\bar{u} + \bar{c}, \bar{u}, \bar{u} - \bar{c}]$, the initial state, which is displayed in Fig. 1, is given by

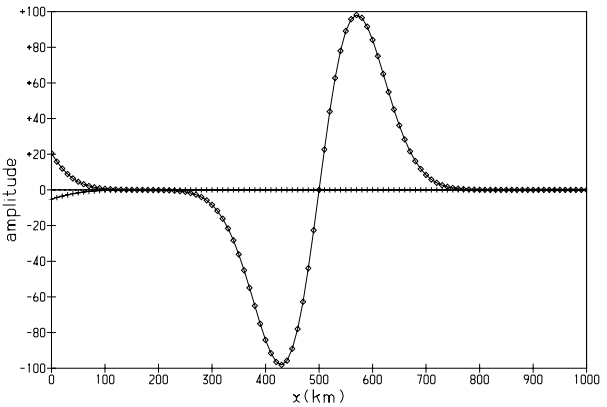

Fig 1. The fields $g\eta$, $\bar{c}u$ and v at time step zero. The field $g\eta$, whose amplitude is given in $m^2\ s^{-2}$ is represented by diamonds; the amplitude of $\bar{c}u$($m^2 s^{-2}$ also) is represented by 'dots'; the amplitude of v (ms^{-1}) is represented by 'plusses'.

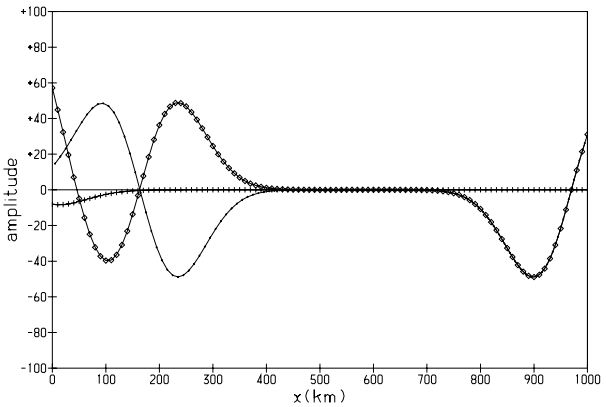

Fig 2. Same as Fig. 1, but after 22.5 min of integration.

$$\eta(x,0) = \left[\breve{Q}^{(0)}_{1,1}\frac{\partial b_1}{\partial t} + \breve{Q}^{(0)}_{1,3}\frac{\partial b_3}{\partial t}\right]\left(x, \frac{L}{2}, 0, \frac{L}{10}\right) + \left[\breve{Q}^{(1)}_{1,2} f b_2\right]\left(x, -\frac{L}{8}, 0, \frac{L}{10}\right),$$

$$u(x,0) = \left[\breve{Q}^{(0)}_{2,1}\frac{\partial b_1}{\partial t} + \breve{Q}^{(0)}_{2,3}\frac{\partial b_3}{\partial t}\right]\left(x, \frac{L}{2}, 0, \frac{L}{10}\right) + \left[\breve{Q}^{(1)}_{2,2} f b_2\right]\left(x, -\frac{L}{8}, 0, \frac{L}{10}\right),$$

$$v(x,0) = \left[\breve{Q}^{(1)}_{3,1} f b_1 + \breve{Q}^{(1)}_{3,3} f b_3\right]\left(x, \frac{L}{2}, 0, \frac{L}{10}\right) + \left[\breve{Q}^{(0)}_{3,2}\frac{\partial b_2}{\partial t}\right]\left(x, -\frac{L}{8}, 0, \frac{L}{10}\right), \quad (42)$$

where $\breve{Q}_{i,j} = n_j Q_{i,j}$. The potential vorticity wave, for example, in eq. (42) is derived by putting $\hat{\mathbf{W}} = (0, s\hat{b}_2, 0)^T$ in eq. (29), dropping terms of higher order than f/s, and performing the inverse Laplace transform. The normalizations n_j were chosen such that the maximum value of η was equal to 10 m both for the shape centred at $x = L/2$ and for the shape centred at at $x = -L/8$. The host initial state was

$$\eta(x^h,0) = \breve{Q}^{(1)}_{1,2} f b_2\left(x^h, \frac{L^h}{2} - \frac{L}{2} - \frac{L}{8}, 0, \frac{L}{10}\right),$$

$$u(x^h,0) = \breve{Q}^{(1)}_{2,2} f b_2\left(x^h, \frac{L^h}{2} - \frac{L}{2} - \frac{L}{8}, 0, \frac{L}{10}\right),$$

$$v(x^h,0) = \breve{Q}^{(0)}_{3,2}\frac{\partial b_2}{\partial t}\left(x^h, \frac{L^h}{2} - \frac{L}{2} - \frac{L}{8}, 0, \frac{L}{10}\right); \quad (43)$$

($x^h = L^h/2$ is the same point in space as $x = L/2$).

Once the integration starts the λ_+-wave will travel toward the boundary at $x = L$ at an approximate velocity of $\bar{u} + \bar{c}$, the λ_--wave will travel toward the boundary at $x = 0$ at an approximate velocity of $\bar{u} - \bar{c}$; simultaneously the λ_{pv}-wave will enter through the boundary at $x = 0$ at an approximate velocity $\bar{u}$. The situation after 22.5 min is displayed in Fig. 2. As can be seen, the centre of the two inertia-gravity waves are at approximately 973 and 163 km as they should be, and the potential vorticity wave has progressed into the area. (These waves will eventually disperse, but they remain recognizable for quite some time.) The integration after 167 min, at which time the incoming potential vorticity wave has travelled approximately 500 km, is shown in Fig. 3. Notice the two gravity-inertia waves have exited without reflection and to the eye the potential vorticity wave has entered the area without distortion and its centre is at 375 km, as it should be. A quantitative measure of the transparency of the boundaries is the fact that after 167 min of integration the rms error for η using the host model forecast as the 'correct answer' is 0.001 m. For comparison, a repeat of this forecast using the boundary conditions $\eta = u = v = 0$, which reflect the inertia-gravity waves and prevent the potential vorticity wave from entering gives a maximum rms error for η of $\sim$3 m. Using these numbers it is fair to argue that the boundaries are more than 99.9% transparent to the incoming potential vorticity wave.

Caveat. It is essential that at $t = 0$ the initial and boundary fields agree. A discontinuity at $x = 0$ will cause η, u and v to drift to unphysical values as the integration proceeds. For example, if the integration described above is repeated with exactly the same boundary conditions and the same initial state *except* for the absence of the tail of the encroaching bell seen at the left-hand edge of Fig. 1, the outcome will be radically different. The introduced discontinuity causes the values of η, u, and v to drift to totally unphysical values. (The boundary conditions are 'working' in the sense that the potential vorticity field defined by eq. (24) enters the area exactly as it should, and the two fields '$\partial(g\eta \pm \bar{u})/\partial t + fv$' exit the area as they should. However they

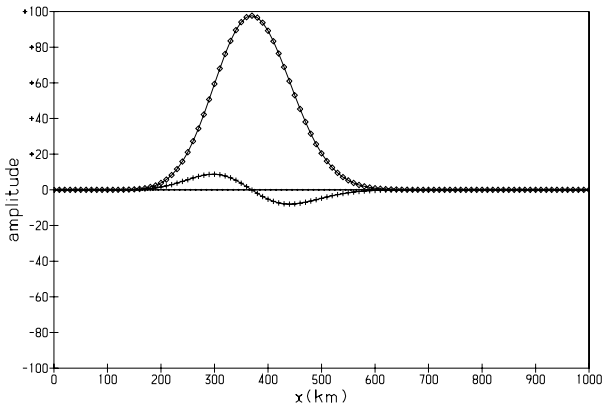

Fig 3. Same as Fig. 1, but after 167 min of integration.

are not working in that the undifferentiated fields η, u, and v drift away to unphysical values.)

3. A multilevel model

In this section (semi)-transparent boundary conditions are derived for a system of equations which supports multiple baroclinic and potential vorticity waves: the two-dimensional linearized hydrostatic primitive equations. A practical demonstration is given of their transparency.

3.1. The equations and their vertical discretization

Gill (1982) gives a description of the approximations involved in arriving at the following linearized set of equations. See Section 7.12 of his book for a discussion of their analytical solutions. The following are his eqs. 7.12.1, 7.12.2, 6.4.6, 6.11.2, and 6.4.3, respectively, with $\partial/\partial y = 0$.

$$\frac{\mathrm{d}u'(x,z,t)}{\mathrm{d}t} + \frac{1}{\rho_0(z)}\frac{\partial p'(x,z,t)}{\partial x} - fv'(x,z,t) = 0, \tag{44}$$

$$\frac{\mathrm{d}v'(x,z,t)}{\mathrm{d}t} + fu'(x,z,t) = 0, \tag{45}$$

$$\frac{\mathrm{d}\rho'(x,z,t)}{\mathrm{d}t} + \frac{\mathrm{d}\rho_0(z)}{\mathrm{d}z}w'(x,z,t) = 0, \tag{46}$$

$$\frac{\partial p'(x,z,t)}{\mathrm{d}z} + g\rho'(x,z,t) = 0, \tag{47}$$

$$\frac{\partial u'(x,z,t)}{\partial x} + \frac{\partial w'(x,z,t)}{\partial z} = 0. \tag{48}$$

In these equations the pressure p', the density ρ', and the x-, y-, and z- components of the winds u', v', and w' are small deviations from an isothermal atmosphere, whose fields are designated by the subscript zero and whose density is $\rho_0(z)$. Lastly,

$$\frac{\mathrm{d}}{\mathrm{d}t} = \frac{\partial}{\partial t} + u_0\frac{\partial}{\partial x}, \tag{49}$$

where u_0 is a constant.

Discretizing in the vertical and defining the ρ'-, u'- and v'-fields on the 'full' levels, and the p'- and w'- fields on the 'half' levels gives rise to the following set of equations. (To reduce typographical clutter later in this section, $p = p'$, $\rho = \rho'$, $u = \rho_0 u'$, $v = \rho_0 v'$, and $w = \rho_0 w'$.)

$$\frac{\mathrm{d}u_m(x,t)}{\mathrm{d}t} + \frac{\partial p_m(x,t)}{\partial x} - fv_m(x,t) = 0; \quad m = 1, M, \tag{50}$$

$$\frac{\mathrm{d}v_m(x,t)}{\mathrm{d}t} + fu_m(x,t) = 0; \quad m = 1, M, \tag{51}$$

$$\frac{\partial u_m(x,t)}{\partial x} + \frac{w_{m+\frac{1}{2}}(x,t) - w_{m-\frac{1}{2}}(x,t)}{\Delta z_m} + \frac{N_m^2}{g}w_m(x,t) = 0; \quad m = 1, M, \tag{52}$$

$$\frac{\mathrm{d}\rho_m(x,t)}{\mathrm{d}t} - \frac{N_m^2}{g}w_m(x,t) = 0; \quad m = 2, M, \tag{53}$$

$$\frac{p_{m+\frac{1}{2}}(x,t) - p_{m-\frac{1}{2}}(x,t)}{\Delta z_m} + g\rho_m(x,t) = 0; \quad m = 2, M, \tag{54}$$

$$\frac{p_{\frac{3}{2}}(x,t) - p_{\frac{1}{2}}(x,t)}{\Delta z_1} + g\rho_2(x,t) = 0, \tag{55}$$

where the Brunt–Väisälä frequency, N^2, is defined in terms of the density of the isothermal atmosphere as

$$N^2(z) = -\frac{g}{\rho_0(z)}\frac{\mathrm{d}\rho_0(z)}{\mathrm{d}z}. \tag{56}$$

The reason there is no ρ_1-field is to eliminate an unwanted computational mode. This is further discussed in Section 3.3.

It is important to emphasize that p_m and w_m are defined by the average of the two adjacent half-levels:

$$p_m \equiv \frac{1}{2}\left[p_{m+\frac{1}{2}} + p_{m-\frac{1}{2}}\right]; \quad w_m \equiv \frac{1}{2}\left[w_{m+\frac{1}{2}} + w_{m-\frac{1}{2}}\right]. \tag{57}$$

Also,

$$\Delta z_m \equiv z_{m+\frac{1}{2}} - z_{m-\frac{1}{2}}. \tag{58}$$

Finally, it is necessary to define boundary conditions at the *top* of the atmosphere, $z_{\frac{1}{2}}$, and at the *bottom* of the atmosphere, $z_{M+\frac{1}{2}}$, where M is the number of full levels. In the absence of orography the physical boundary condition at the bottom is

$$w_{M+\frac{1}{2}} = 0. \tag{59}$$

At the top of the atmosphere the boundary condition $w_{\frac{1}{2}} = 0$ kills the external mode; see Kalnay (2003), p. 46. Consequently, a material boundary is used at the top in order to retain this mode:

$$\frac{\mathrm{d}p_{\frac{1}{2}}(x,t)}{\mathrm{d}t} - gw_{\frac{1}{2}}(x,t) = 0. \tag{60}$$

Defining $a_m^{\pm} = [1 \pm \Delta z_m\, N_m^2/(2g)]$, multiplying eq. (52) by Δz_m, and summing over m yields a recursive relation for $w_{m-\frac{1}{2}}$:

$$w_{m-\frac{1}{2}}(x,t) = \frac{1}{a_m^-}\left(\Delta z_m\frac{\partial u_m(x,t)}{\partial x} + a_m^+ w_{m+\frac{1}{2}}(x,t)\right), \tag{61}$$

which, combined with the definition of w_m in eq. (57), facilitates the replacement of eq. (52) with the following two equations:

$$w_m(x,t) = -\frac{g}{N_m^2}\sum_{j=1}^{M}\tau_{m,j}\frac{\partial u_j(x,t)}{\partial x}, \tag{62}$$

$$w_{\frac{1}{2}}(x,t) = -\frac{1}{g}\sum_{j=1}^{M}\nu_j\frac{\partial u_j(x,t)}{\partial x}. \tag{63}$$

The matrix $\boldsymbol{\tau}$ and the transposed vector $\boldsymbol{\nu}$ are functions of Δz, N^2, and g only. Although algebraically complicated they are rather easy to generate in a computer program because of their recursiveness. The factors in front of eqs. (62) and (63) are included to make eqs. (73) and (74) look more elegant.

Multiplying eq. (55) by Δz_1 and using the definition of p_m in eq. (57) yields

$$p_1 = p_{\frac{1}{2}} - g\frac{\Delta z_1}{2}\rho_2. \tag{64}$$

Multiplying eq. (54) by Δz_m and summing from the top down results in

$$p_m = p_{\frac{1}{2}} - g\left(\frac{\Delta z_m}{2}\rho_m + \sum_{j=2}^{m-1}\Delta z_j\rho_j + \Delta z_1\rho_2\right); \quad m = 2, M \tag{65}$$

and

$$p_{M+\frac{1}{2}} = p_{\frac{1}{2}} - g\left(\sum_{j=2}^{M}\Delta z_j\rho_j + \Delta z_1\rho_2\right). \tag{66}$$

If a field ρ_1 is defined such that

$$-g\Delta z_1\rho_1 = p_{\frac{1}{2}} - g\Delta z_1\rho_2, \tag{67}$$

then eqs. (64)–(66) can be written as

$$\mathbf{p} = \boldsymbol{\Gamma}\boldsymbol{\rho}, \tag{68}$$

$$p_{M+\frac{1}{2}} = \boldsymbol{\eta}\cdot\boldsymbol{\rho}, \tag{69}$$

where $\boldsymbol{\Gamma}$ is a square matrix defined by the relationships

$$p_1(x,t) = -g\Delta z_1\left(\rho_1 - \frac{1}{2}\rho_2\right), \tag{70}$$

$$p_m(x,t) = -g\left(\frac{\Delta z_m}{2}\rho_m + \sum_{j=1}^{m-1}\Delta z_j\rho_j\right); \quad m = 2, M, \tag{71}$$

and where $\boldsymbol{\eta}$ is a transposed vector defined by

$$p_{M+\frac{1}{2}} = -g\sum_{j=1}^{M}\Delta z_j\rho_j. \tag{72}$$

It is important to emphasize that ρ_1 is *not* the density at level 1. The reason for its introduction is to restructure eqs. (64)–(66) into a form which lends itself to formal matrix manipulation.

Using eqs. (62) and (63), eqs (53) and (60) can be written as

$$\frac{\mathrm{d}\rho_m(x,t)}{\mathrm{d}t} + \sum_{j=1}^{M}\tau_{m,j}\frac{\partial u_j(x,t)}{\partial x} = 0; \quad m = 2, M, \tag{73}$$

and

$$\frac{\mathrm{d}p_{\frac{1}{2}}(x,t)}{\mathrm{d}t} + \boldsymbol{\nu}\cdot\frac{\partial\mathbf{u}(x,t)}{\partial x} = 0. \tag{74}$$

To solve the equations of motion in the interior eqs. (50), (51), (73), and (74) are used to update u_m and v_m for $m = 1, M$, ρ_m for $m = 2, M$, and $p_{\frac{1}{2}}$, respectively. Then eq. (67) is used to update ρ_1, which is then used in eq. (68) to update $\mathbf{p}$.

3.2. The boundary conditions

To derive the boundary conditions one proceeds as follows. Take $\mathrm{d}/\mathrm{d}t$ of eq. (67) and substitute the resulting $\mathrm{d}p_{\frac{1}{2}}/\mathrm{d}t$ in eq. (74). Combining the result with eq. (73) one arrives at the equation

$$\frac{\mathrm{d}\boldsymbol{\rho}(x,t)}{\mathrm{d}t} + \check{\boldsymbol{\tau}}\frac{\partial\mathbf{u}(x,t)}{\partial x} = 0, \tag{75}$$

where for any vector $\mathbf{D} = (D_1, D_2, \ldots\ D_M)^T$,

$$(\check{\boldsymbol{\tau}}\boldsymbol{D})_1 = (\boldsymbol{\tau}\boldsymbol{D})_2 - \frac{1}{g\Delta z_1}\boldsymbol{\nu}\cdot\boldsymbol{D}; \quad (\check{\boldsymbol{\tau}}\boldsymbol{D})_m \equiv (\boldsymbol{\tau}\boldsymbol{D})_m, m = 2, M. \tag{76}$$

Taking $\mathrm{d}/\mathrm{d}t$ of eq. (68) and substituting the result in $\boldsymbol{\Gamma}$ times eq. (75) results in

$$\frac{\mathrm{d}\mathbf{p}(x,t)}{\mathrm{d}t} + \boldsymbol{\Gamma}\check{\boldsymbol{\tau}}\frac{\partial\mathbf{u}(x,t)}{\partial x} = 0. \tag{77}$$

Assume there exists a matrix $\mathbf{E}$ which diagonalizes $\boldsymbol{\Gamma}\check{\boldsymbol{\tau}}$:

$$\mathbf{E}^{-1}\boldsymbol{\Gamma}\check{\boldsymbol{\tau}}\boldsymbol{E} = \mathbf{C}^{\mathbf{2}}, \tag{78}$$

where the diagonal matrix has been written as $\mathbf{C}^2$ for later convenience. The diagonal elements are defined as $C_{m,m} = c_m$. Using eq. (78), eqs. (77), (50) and (51) can be re-written as

$$\frac{\mathrm{d}(\mathbf{E^{-1}p})_m}{\mathrm{d}t} + c_m^2\frac{\partial(\mathbf{E^{-1}u})_m}{\partial x} = 0, \tag{79}$$

$$\frac{\mathrm{d}(\mathbf{E^{-1}u})_m}{\mathrm{d}t} + \frac{\partial(\mathbf{E^{-1}p})_m}{\partial x} - f(\mathbf{E^{-1}v})_m = 0, \tag{80}$$

$$\frac{\mathrm{d}(\mathbf{E^{-1}v})_m}{\mathrm{d}t} + f(\mathbf{E^{-1}u})_m = 0. \tag{81}$$

For each $m = 1, M$ eqs. (79)–(81) are formally identical to eqs. (1)–(3). Therefore, the method derived for generating the semi-transparent boundary fields in Section 2 can be applied to derive $\mathbf{E}^{-1}\mathbf{p}$, $\mathbf{E}^{-1}\mathbf{u}$ and $\mathbf{E}^{-1}\mathbf{v}$ at the boundaries, from which $\mathbf{u}$, $\mathbf{v}$, and $\mathbf{p}$ at the boundaries follow trivially. Thereafter $\boldsymbol{\rho}$ at the boundary is derived by operating on eq. (68) with $\boldsymbol{\Gamma}^{-1}$, which, in turn allows the computation of the boundary values of $p_{\frac{1}{2}}$ via eq. (67).

3.3. The vertical distribution of the fields

The purpose of this section is to answer the question: why the inelegant choice of having no ρ_1-field in eqs. (53)–(55)? To answer this consider what would have happened if this field had

been retained. Using the same derivation as in Section 3.1, then instead of eq. (65), the following relationship between $\mathbf{p}$ and $\boldsymbol{\rho}$ would have resulted:

$$p_m = p_{\frac{1}{2}} - g\left(\frac{\Delta z_m}{2}\rho_m + \sum_{j=1}^{m-1}\Delta z_j \rho_j\right); \tag{82}$$

see eqs. (3.22) and (3.23) of M05. Also, instead of eq. (77) the following equation would have been derived:

$$\frac{\mathrm{d}\mathbf{p}(x,t)}{\mathrm{d}t} + \mathbf{M}\frac{\partial \mathbf{u}(x,t)}{\partial x} = 0, \tag{83}$$

where the $M \times M$ matrix $\mathbf{M}$ is defined in M05. We then would have proceeded as described in section 3.2 to derive semi-transparent boundary conditions for the $3 \times M$ fields $\mathbf{u}$, $\mathbf{v}$ and $\mathbf{p}$. Now there would be a problem: $M + 1$ boundary fields, ($\rho_m, m = 1, M,$ *and* $p_{\frac{1}{2}}$) would be needed in order to continue with the integration, but there are only M values of $\mathbf{p}$ available for their computation. That is, eq. (82) could not be inverted because it is under determined.

This is a well-known problem associated with this vertical distribution of the fields, and normally some physical assumption, which is not appropriate for deriving transparent boundary conditions, is made to provide the extra piece of information. See, for example 'step c' on page 108 of Daley (1979) for his physical assumption, made in the context of normal mode initialization.

Looking at eq. (82), it will become invertible if any one of the ρ_m fields is removed. If this is done one arrives at a relation, eq. (68), which can be solved for $\boldsymbol{\rho}$ without any additional assumptions. Equation (67) then yields $p_{\frac{1}{2}}$. (The choice of removing ρ_1 was made on the basis of mathematical convenience, see eq. (76), and physical reasoning: if two layers of the model must have the same density anomaly, then in a meteorological model the top two layers are almost certainly the best choice.)

One may ask the question: how was this problem avoided in M05? The answer is that for the gravity waves there is an additional condition, which can be seen by writing eq. (A9) of M05 in the more elegant form

$$\frac{\mathrm{d}}{\mathrm{d}t}(\boldsymbol{\tau}^{-1}\boldsymbol{\rho} - \mathbf{M}^{-1}\mathbf{p}) = 0, \tag{84}$$

which permits the computation of $\boldsymbol{\rho}$ if $\mathbf{p}$ is known:

$$\boldsymbol{\rho} = \boldsymbol{\tau}\mathbf{M}^{-1}\mathbf{p}. \tag{85}$$

However, when the Coriolis terms are included there is a subtle change: the equations now support additional solutions, the 'slow' (potential vorticity) waves. These waves have the property that $\mathrm{d}\psi/\mathrm{d}t = 0$ for any field ψ. As a result, eq. (84), which still holds when the Coriolis terms are present, does not give an additional relationship between $\boldsymbol{\rho}$ and $\mathbf{p}$.

3.4. Testing the boundary conditions

In this section a practical demonstration is given of the transparency of the boundary conditions derived in Section 3.2. First, it is shown that the boundary conditions work well for outgoing potential vorticity waves. Second, it is shown that they are transparent to an externally imposed incoming potential vorticity wave: it enters almost without distortion. Lastly, it is shown that the slowest gravity wave, for which $\bar{u}/\bar{c} \approx 10$ and thus for which the assumption that f^2/s^2 can be regarded as a small quantity is under the most strain (see eq. 15), exits the area with minimal reflection.

The horizontal spatial discretization of eqs. (50), (51), (73), and (74) is the same as that for eqs. (38)–(40) with the fields ρ_m, p_m and $p_{\frac{1}{2}}$ being discretized as are the η fields there. A Robert (1966) filter is used to control the computational mode.

For an isothermal atmosphere $N^2 = g^2/(RT_0)$. The value $T_0 = 250$ K was used; $R = 287.04$ J kg^{-1} K^{-1}. For the discretization, $\Delta x = 10$ km, $\Delta t = 9.0$ s, $z_{\frac{1}{2}} = 10$ km; $M = 10$ and the levels are equally spaced; thus $\Delta z_m = -1$ km. These result in $c_1 = 281.5$, $c_2 = 100.5$, $c_3 = 54.6$, $c_4 = 36.1$, $c_5 = 25.5$, $c_6 = 18.3$, $c_7 = 12.9$, $c_8 = 8.6$, $c_9 = 5.0$, $c_{10} = 1.6$, all of these having units of ms^{-1}. The impact of changing the treatment of the density in the top layer can be seen by comparing these velocities with those in M05. The advecting velocity was chosen to be $u_0 = 25$ ms^{-1}.

The matrices $\mathbf{Q}_{\mathrm{m}}^{-1}$ and $\mathbf{Q}_{\mathrm{m}}$ used in this section are defined by eqs. (26) and (27), respectively, with $\bar{c}$ replaced by c_m, and $\bar{u}$ replaced by u_0. Also, the gravity-inertia wave solution whose velocity is $u_0 \pm c_m$ will be called the '$\{m\}_{\pm}$-wave', and the corresponding potential vorticity wave the '$\{m\}_{pv}$-wave'.

Two sets of integrations were performed; one with $L = 1000$ km, $I = 101$, and a second 'host integration' with $L^h = 10\,000$ km, and $I^h = 1001$. The latter integration furnished the correct forecast for measuring the errors for all three tests that follow and also the boundary fields describing and the incoming waves in test 2 below.

To measure the error for any field ψ, the root mean square difference between the fields ψ^n and $(\psi^h)^n$ was computed at each time step n. To measure the relative magnitude of this error it was divided by the root mean square difference between the $(\psi^h)^n$ and zero at time N:

$$R^n(\psi) = \left[\sum_{i=1}^{I}\sum_{k=1}^{M}\left\{(\psi^h)_{i,k}^n - \psi_{i,k}^n\right\}^2\right]^{\frac{1}{2}} \div \left[\sum_{i=1}^{I}\sum_{k=1}^{M}\left\{(\psi^h)_{i,k}^N\right\}^2\right]^{\frac{1}{2}}. \tag{86}$$

N differs from test to test because the denominator only makes sense in these tests when the 'shape' is inside the integration area and it will be chosen judiciously depending on the test being performed.

Test 1. Do the potential vorticity waves exit without reflection?

To see whether the potential vorticity waves exited without reflection the following pure $\{m\}_{pv}$-wave, centred at $L/2$, was

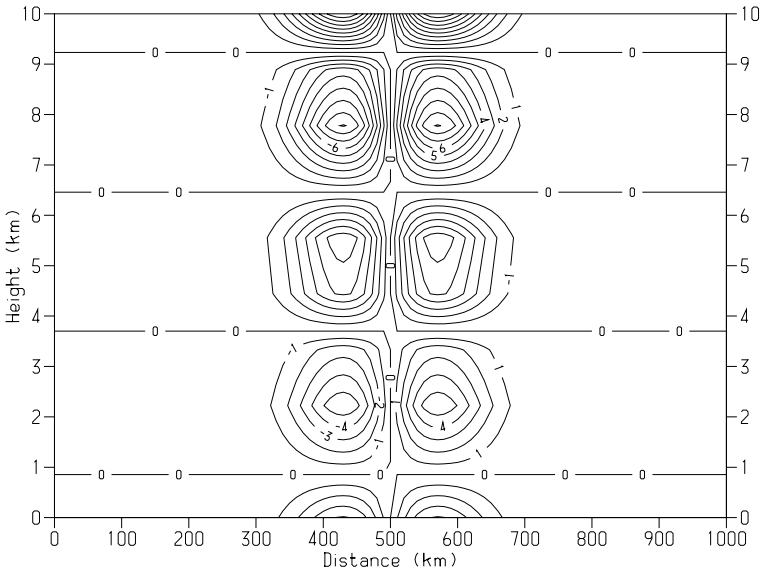

Fig 4. The wind anomaly v' for the $\{5\}_{pv}$-wave at the initial time.

used as an initial state:

$$p_j(x,0) = E_{j,m}[\breve{Q}_m]^{(1)}_{1,2} f b_2\left(x, \frac{L}{2}, 0, \frac{L}{10}\right),$$

$$u_j(x,0) = E_{j,m}[\breve{Q}_m]^{(1)}_{2,2} f b_2\left(x, \frac{L}{2}, 0, \frac{L}{10}\right),$$

$$v_j(x,0) = E_{j,m}[\breve{Q}_m]^{(0)}_{3,2} \frac{\partial b_2}{\partial t}\left(x, \frac{L}{2}, 0, \frac{L}{10}\right), \qquad (87)$$

where $[\breve{Q}_m]_{i,2} = n_2[Q_m]_{i,2}$. The normalization n_2 was chosen such that the maximum value of $|v'_m(x,0)| = 10\,\mathrm{ms}^{-1}$; (recall that $\rho_0 v' = v$). The field $v_5(x,0)/\rho_0$ is displayed in Fig. 4. Once the integration began this shape moved toward the boundary at $x = L$ with a velocity of 25 ms^{-1}. Because the shape is approximately 400 km wide, see Fig. 4, it took about 7.8 h for the bulk of it to clear the area; (700 km at 25 ms^{-1}).

In order to make this test meaningful the host model fields were used *solely* to measure the rms errors. Thus, in using eq. (28) the $\hat{\mathbf{W}}$ were chosen as follows for each mode $m = 1, 5$: at $x = 0$, $\hat{\mathbf{W}} = (0, 0, \hat{W}^g_3)^T$ and at $x = L$, $\hat{\mathbf{W}} = (\hat{W}^g_1, \hat{W}^g_2, 0)^T$; and as follows for each mode $m = 6$, 10: at $x = 0$, $\hat{\mathbf{W}} = (0, 0, 0)^T$ and at $x = L$, $\hat{\mathbf{W}} = (\hat{W}^g_1, \hat{W}^g_2, \hat{W}^g_3)^T$.

The error caused by any reflection at $x = L$ was measured using $R^n(v)$ with $N = 0$, with which value the denominator is an excellent measure of the size of the phenomenon being modelled. By definition $R^0(v) = 0$. Also, if this wave were fully reflected at $x = L$ then subsequently $R^n(v)$ would equal 1. Equally, $R^n(v)$ would subsequently equal zero if the wave exited without reflection. In fact, for the initial state displayed in Fig. 4, $R^n(v)$ remained at zero until the front edge of the wave struck the boundary and slowly rose to a final value of 1% after the wave exited. Subsequent to that $R^n(v)$ was constant until the bulk of the reflected wave was transmitted through the boundary at $x = 0$, which caused $R^n(v)$ to fall further to a value of 0.1%. The same test was carried out for each of the other $\{m\}_{pv}$-waves, using initial fields as described by eq. (87). For each integration $R^n(v)$ subsequent to the exit of the shape was approximately the same size, the largest value being $R^n(v) = 1.3\%$ for the $\{10\}_{pv}$-wave.

Test 2. Are the boundaries transparent for incoming potential vorticity waves?

The purpose of this experiment is to show that potential vorticity waves from an external source can be injected accurately into the integration area. Thus it is assumed that a $\{5\}_{pv}$ wave, initially centred outside the area at $x = -2L/5$, crosses the boundary at $x = 0$ during the integration, moving at a velocity of 25 ms^{-1}. Can the boundary conditions derived in Section 3.2 accurately model this scenario?

To generate the boundary fields a forecast was run on the host area with the initial state described by eq. (87) with x replaced with x^h and $L/2$ replaced with $L^h/2 - L/2 - 2L/5$. This was integrated for 9 h, at which time the $\{5\}_{pv}$ wave was centred at $x^h = L^h/2 - 90$ km, well inside the guest integration area. The fields $\boldsymbol{\rho}^h$, $\mathbf{u}^h$, $\mathbf{v}^h$ and $p^h_{\frac{1}{2}}$ at $x^h = L^h/2 - L/2 + \Delta x/2$ were computed at every time step and written to a file. During the guest forecast these fields were read in at each time step and used to compute the boundary fields for each mode, m, using eq. (33).

$R^n(v)$ with N chosen as the last step in the forecast was used to measure the transparency of the boundary at $x = 0$. At time step N the bulk of the shape was inside the integration area, see Fig. 5, making the denominator in eq. (86) a good measure of the size of the phenomenon being measured. $R^0(v) = 0$ by definition, and $R^n(v) = 0$ for an external wave that enters perfectly; also, $R^n(v) = 1$ for a wave that fails totally to be transmitted through the inflow boundary.

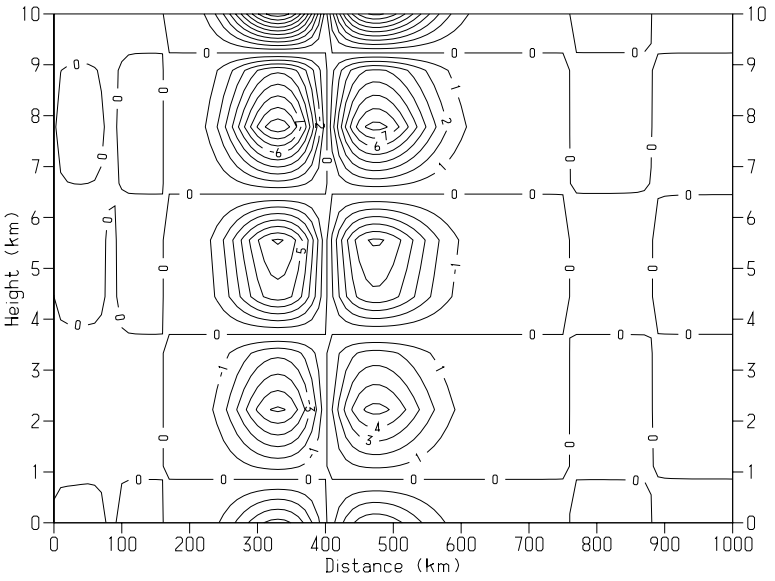

Fig 5. The wind anomaly v' for the injected $\{5\}_{pv}$-wave after 9 h of integration.

The similarity of Fig. 5 to Fig. 4 is an indication that the wave has been transmitted accurately through the boundary, a fact confirmed by the value of $R^N(v) = 0.04\%$.

Test 3. Are the boundaries still transparent for outgoing gravity waves?

The basis for deriving semi-transparent boundary conditions is the assumption that f/s can be regarded as a small parameter. From eqs. (15) and (17) it is clear that this assumption is tested most severely for waves such that $u_0/c_m \gg 1$. Therefore, the question addressed by this test is: how transparent is the boundary at $x = L$ to an outgoing $\{10\}_+$-wave, for which $u_0/c_{10} = 15.6$? The initial state, situated at $L/2$ is

$$p_j(x,0) = E_{j,m}[\breve{Q}_m]^{(0)}_{1,1}\frac{\partial b_1}{\partial t}\left(x, \frac{L}{2}, 0, \frac{L}{10}\right),$$

$$u_j(x,0) = E_{j,m}[\breve{Q}_m]^{(0)}_{2,1}\frac{\partial b_1}{\partial t}\left(x, \frac{L}{2}, 0, \frac{L}{10}\right),$$

$$v_j(x,0) = E_{j,m}[\breve{Q}_m]^{(1)}_{3,1} f b_1\left(x, \frac{L}{2}, 0, \frac{L}{10}\right), \tag{88}$$

with $m = 10$; see Fig. 6. The fields are normalized such that u' is 10 ms^{-1}. On starting the integration this wave moves in the $+x$-direction with a velocity of approximately 26.6 ms^{-1}.

In order to make this test meaningful the host model fields were used *solely* to measure the rms errors. Thus, in using eq. (28) the $\hat{\mathbf{W}}$ were chosen as follows for each mode $m = 1, 5$: at $x = 0$, $\hat{\mathbf{W}} = (0, 0, \hat{W}^g_3)^T$ and at $x = L$, $\hat{\mathbf{W}} = (\hat{W}^g_1, \hat{W}^g_2, 0)^T$; and as follows for each mode $m = 6, 10$: at $x = 0$, $\hat{\mathbf{W}} = (0, 0, 0)^T$ and at $x = L$, $\hat{\mathbf{W}} = (\hat{W}^g_1, \hat{W}^g_2, \hat{W}^g_3)^T$.

The error caused by any reflection at $x = L$ was measured using $R^n(u)$ with $N = 0$, at which time the denominator is an excellent measure of the size of the phenomenon being modelled. By definition $R^0(u) = 0$. Also, if this wave were fully reflected at $x = L$ then subsequently $R^n(u)$ would equal 1. Equally, $R^n(u)$ would subsequently equal zero if the wave exited without reflection. In fact, $R^n(u)$ remained at zero until the front edge of the wave struck the boundary and slowly rose to a final value of 2.2% as the wave exited. Subsequent to that $R^n(u)$ oscillated between 1.3% and 2.2%. The integration is stable but the presence of the dispersion does reduce the transparency of the boundary a little.

4. Conclusion

The objective of this paper was to demonstrate that the approach to open boundaries advocated by Engquist and Majda (1977) is sufficiently robust to accommodate potential vorticity waves when baroclinic waves are also present. For the single-layer model a transparency of the boundaries of better than 99% was demonstrated. For the multilevel model the results were also encouraging. For outgoing potential vorticity waves a transparency of better than 98.7% was demonstrated, and for incoming potential vorticity waves a transparency of 99.9% was demonstrated. Equally important, the boundaries were shown to be stable and 97.8% transparent for the potentially most troublesome slowest gravity-inertia waves.

In Section 2 it was shown that the derived boundary conditions caused the fields to drift to unphysical values if the boundary fields at time zero did not agree with the initial fields on the boundary. By implication, if at any time during the integration a jump discontinuity is introduced at the boundary the fields can be expected to drift to unphysical values during the remainder of the integration. Therefore, for these boundary conditions to work in a more realistic nested setting, in which the host model time and space discretizations differ from those of the guest model, it is essential that the space and time interpolation of the fields

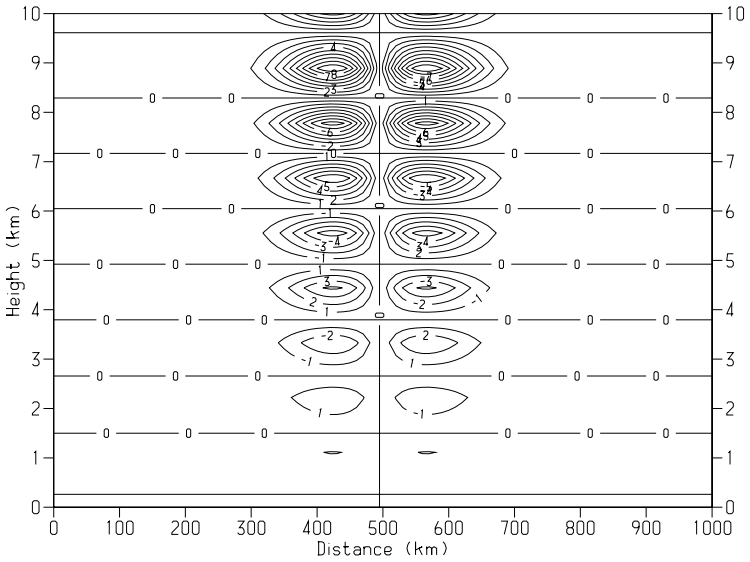

Fig 6. The wind anomaly u' for the $\{10\}_+$-wave at the initial time.

from the host grid to the guest grid produce well-behaved fields. (McDonald, 2003, gives a practical demonstration of a forecast being improved by increasing the smoothness of the boundary fields.) Termonia (2004) has demonstrated that the time interpolation of the host fields can be controlled by estimating the noise due to that interpolation by means of a digital filter.

In this paper it has been demonstrated that potential vorticity waves can be injected into a nested model while simultaneously allowing gravity waves to exit with minimal reflection for a two-dimensional linear system of equations which supports multiple baroclinic and potential vorticity waves. It is a big step from there to an operational set-up involving a three-dimensional system of non-linear equations, including orography and physical parameterization schemes. Since the derivation of transparent boundary conditions presupposes the fields are mathematically smooth, a well-initialized set of analysed fields would seem to be a prerequisite to them working in this more challenging environment. Their derivation also assumed flat orography. Relaxing this assumption will generate non-constant wave speeds for the normal modes. It will be interesting whether this will be a minor irritant (possibly resulting in slightly larger reflection from the boundary) or a major stumbling block (causing boundary instability, for example).

5. Acknowledgments

Thanks to Jim Hamilton for help with the graphics. Thanks to the HIRLAM group for their support and encouragement. The helpful criticism of two anonymous reviewers is also much appreciated.

References

Daley, R. 1979. An application of non-linear normal mode initialization to an operational forecast model. *Atmos. Ocean* **17**, 97–124.

Doetsch, G. 1971. In: *Guide to the Application of the Laplace and Z-Transforms*, Van Nostrand Reingold Co., 240pp.

Engquist, B. and Majda, A. 1977. Absorbing boundary conditions for the numerical simulation of waves. *Math. Comput.* **31**, 629–651.

Gill, A. E. 1982. In: *Atmosphere-Ocean Dynamics*. Academic Press, 662pp.

Hagstrom, T. 1999. Radiation boundary conditions for the numerical simulation of waves. *Acta Numerica* **8**, 47–106.

Ince, E. L. 1956. In: *Ordinary Differential Equations*. Dover, 558pp.

Kalnay, E. 2003. In: *Atmospheric Modeling, Data Assimilation, and Predictability*. Cambridge University Press, 341pp

McDonald, A. 2002. A step toward transparent boundary conditions for meteorological models. *Mon. Wea. Rev.* **130**, 140–151.

McDonald, A. 2003. Transparent boundary conditions for the shallow water equations: testing in a nested environment. *Mon. Wea. Rev.* **131**, 698–705.

McDonald, A. 2005. Transparent lateral boundary conditions for baroclinic waves: a study of two elementary systems of equations. *Tellus* **57A**, 171–182.

Robert, A. 1966. The integration of a low order spectral form of the primitive meteorological equations. *J. Meteor. Soc. Japan* **44**, 237–245.

Termonia, P. 2004. Monitoring the coupling-update frequency of a limited-area model by means of a recursive digital filter. *Mon. Wea. Rev.* **132**, 2130–2141.